This is an Accepted Manuscript of Yu, T., Mangalvedhe, K., Francoeur, M., and Bergthorson, J. M. (2024), Dual-range emission spectroscopy for temperature measurement of laminar aluminum dust flames, Combustion and Flame 263. doi: 10.1016/j.combustflame.2024.113421. Licensed under CC BY-NC-ND

Dual-range emission spectroscopy for temperature measurement of laminar aluminum dust flames

Tao Yu*, Kartik Mangalvedhe, Mathieu Francoeur, Jeffrey M. Bergthorson

Department of Mechanical Engineering, McGill University, 817 Sherbrooke Street West, Montréal, Québec, H3A 0C3, Canada

Abstract

Understanding the temperature fields/profiles in aluminum dust flames is critical to the design of aluminum-based sustainable fuels and the development of aluminum combustion simulation tools. Although emission spectroscopy has been applied in aluminum flames, the signals in most works were integrated along the recording path and over the whole flame and, therefore, the measurements could not provide information of the flame spatial structure. In addition, the details of the diagnostic method were scarcely introduced. This work develops a dual-range emission spectroscopy diagnostic system for 1D measurements of the liquid temperature and the flame temperature of aluminum flames. The important aspects for diagnostics, such as the instrument specifications, signal acquisition strategy, data processing, accuracy and precision, are introduced and quantified in detail. The continuous spectrum from the liquid phase of $Al_{(L)}$ and/or $Al_2O_{3(L)}$, rovibrational AlO spectrum from the micro-diffusion flame, and 2D flame luminosity are recorded simultaneously. Based on Planck's law, a linear fitting method is implemented to derive a continuous spectrum temperature. A nonlinear minimization framework based on the stick spectrum is introduced to fit the AlO spectra and derive a AlO temperature. The accuracy and precision are quantified by a comparison of the average temperatures against the equilibrium temperatures and the standard deviations. The effectiveness of this technique for temperature measurements of aluminum dust flames is verified by the agreement of the continuous spectrum temperature and the AlO temperature in the post-flame region. The 1D distribution of the continuous spectrum temperature indicates the boiling of Al and the dissociation/condensation of Al_2O_3 from upstream to downstream through the flame. The 1D temperature distributions also present a lag of the continuous spectrum temperature compared to the AlO

This is an Accepted Manuscript of Yu, T., Mangalvedhe, K., Francoeur, M., and Bergthorson, J. M. (2024), Dual-range emission spectroscopy for temperature measurement of laminar aluminum dust flames, Combustion and Flame 263. doi: 10.1016/j.combustflame.2024.113421. Licensed under CC BY-NC-ND

temperature, indicating that the continuous spectrum temperature is dominated by the Al fuel droplets and the Al_2O_3 caps, instead of the Al_2O_3 nanometric droplets.

Key words: aluminum dust flame; emission spectroscopy; temperatures; 1D diagnostics

Novelty and Significance of Statement

Metal fuels have come into spotlight due to their promise for reducing carbon emissions as they can be recycled from their combustion products with green electricity. Among proposed metal fuels, aluminum is characterized by a very high energy density. Although there are many works on aluminum dust flames in the past decades, the structure of aluminum dust flames still remains unclear. This is due to the diagnostic challenges of aluminum dust flames caused by the large interference of flame luminosity, the optical thickness effect, and the multi-phase medium that leads to light scattering and both micro and macro temperature gradients. This work develops a dual-range emission spectroscopy technique with the aim of measuring liquid temperature and flame temperature. The instrument specifications, signal acquisition strategy, data processing, accuracy and precision of the diagnostic system are introduced and quantified clearly. The 1D temperature distributions through the aluminum flame front suggest the presence of the boiling of Al and the dissociation of Al_2O_3 from upstream to downstream through the flame, and present a lag of the continuous spectrum temperature compared to the AlO temperature. This lag indicates that the continuous spectrum temperature is dominated by the Al fuel droplets and the Al_2O_3 caps, instead of the Al_2O_3 nanometric droplets. The findings presented by the spatial temperatures will be of great interest to the metal combustion community, and particularly to researchers working on aluminum flame models.

Author Contributions

Tao Yu and Kartik Mangalvedhe conceived the idea and conducted the experiments. Tao Yu designed the diagnostic system and performed the data analysis. Kartik Mangalvedhe, Mathieu Francoeur and Jeffrey M. Bergthorson discussed the data analysis. Jeffrey M. Bergthorson supervised the project. Tao Yu wrote the manuscript. All authors discussed the results, assisted with the manuscript preparation and revised the manuscript.

This is an Accepted Manuscript of Yu, T., Mangalvedhe, K., Francoeur, M., and Bergthorson, J. M. (2024), Dual-range emission spectroscopy for temperature measurement of laminar aluminum dust flames, Combustion and Flame 263. doi: 10.1016/j.combustflame.2024.113421. Licensed under CC BY-NC-ND

1. Introduction

In order to address the issues associated with global climate change and energy crises, the development of sustainable, zero-carbon, non-polluting fuels is a key priority [1, 2]. Micron-sized metal powders are promising alternative fuels because their combustion products are mainly metal oxide(s), which are solid particles that can be collected and reduced back into metals using sustainable energy [3]. In addition, metal fuels are characterized by high energy densities, and possess broad applications in propulsion, explosive, electrical and thermal power generation. However, metal flames involve complicated physical processes and chemical reactions, such as evaporation, condensation, combustion, radiation heat transfer between fuel particles/droplets, flames, gas phase, and products, which are not well-understood. Further understanding of metal flames requires advanced optical diagnostics for the measurement of species concentration, temperature, particle size, and burning velocity [4-7].

The application of optical diagnostics for the measurements of species and temperature in metal flames is challenging due to the strong flame luminosity and the potential of optical thickness effect. The strong flame luminosity caused by thermal emission at high temperature, *e.g.*, between 3000 K and 3500 K for aluminum flames [8, 9] can result in large interference for the laser diagnostics, such as laser-induced fluorescence (LIF) and Raman spectroscopy [10, 11]. Past works have demonstrated that LIF for Al atom and AlO molecule is applicable for aluminum particles burning in combustion chambers [12, 13]. Possibly due to the attenuation effect by large particles (~230 μm), a relatively powerful laser was used by Bucher *et al.* [12] to excite LIF-AlO. The laser energy was in excess of 40 mJ/pulse, corresponding to a fluence that could heat up the particles to a temperature above the boiling point of aluminum [14]. Aluminum may transition into vapor because of the laser interaction. This impacts the aluminum flame, and laser interaction may become intense for small aluminum particles used in dust flames due to their small heat capacities. Until now, LIF has not been applied to aluminum dust flame. These anticipated issues need to be assessed in experiments. Laser induced phosphorescence that can measure combustible temperature (below 1000 K) and surface temperature [15, 16] is not suitable for metal flames since the phosphorescent material can be decomposed at metal flame temperatures. Laser induced incandescence (LII) that is commonly used to measure primary particle diameter for sooty flames is also likely not applicable for metal flames. The reason is that the pulsed laser can heat the particles up to ~4000 K [17], exceeding the melting, boiling or ignition points of most metals and their oxide(s) that can destroy the original combustion condition. Although the measurements of particle

This is an Accepted Manuscript of Yu, T., Mangalvedhe, K., Francoeur, M., and Bergthorson, J. M. (2024), Dual-range emission spectroscopy for temperature measurement of laminar aluminum dust flames, Combustion and Flame 263. doi: 10.1016/j.combustflame.2024.113421. Licensed under CC BY-NC-ND

size distribution have been reported using digital in-line holography [18], it is problematic for metal dust flames. This is because the particles are too small and dense such that 1) the multiple neighbouring interference fringes are coupled together; 2) the single interference fringe cannot be identified in the image due to the small size of the interference pattern. If two laser beams are available, holographic interferometry can be established and applied in metal flames to calculate the temperature distribution [19]. However, this technique requires the implementation of Abel transform to obtain the radial distribution of the refraction index, and is therefore only applicable to axisymmetric flames. Additionally, the calculation is conducted based on the distribution of refractive index of the non-reacting medium, which is unknown and difficult to obtain. In addition, the signal-to-noise ratio (SNR) is a concern since the interference signals can be attenuated due to the optical thickness of the medium. Laser absorption spectroscopy seems to be a promising technique, but more efforts are still required. Soo *et al.* [20] performed absorption spectroscopy for the Al I atomic lines to provide a realistic measurement of the aluminum vapor in the pre-heat and combustion zones. However, this work only provides qualitative measurement, and such a technique is not able to resolve aluminum concentration or temperature. Ruesch *et al.* [21] and Zhang *et al.* [22] demonstrated that quantitative measurement for species concentration and temperature is feasible for propellant flames by using absorption spectroscopy for CO and H_2O. This suggests the potential application of absorption spectroscopy for metal dust flames if a sophisticated strategy is developed to address the difficulties concerning signal attenuation, beam steering, etc.

Emission spectroscopy may be the most suitable method for metal flames due to its ease of implementation and little concerns from laser interference. Goroshin *et al.* [8] performed a pioneering work of emission spectroscopy by using an optical fiber spectrometer for both the continuous spectrum and the AlO spectrum. The line-of-sight (LOS) measurements were reversed by using the Abel transform, based on which 1D distributions of a condensed emitter temperature and an AlO temperature were determined. It was found that the two temperatures coincide with each other and are 100-200 K lower than the equilibrium flame temperature. However, the size of the field of view and the LOS integrated path are difficult to determine when optical fiber spectrometer is used to acquire the signals. Furthermore, the LOS measurement would overestimate the temperature since signals not originating from a perfect focus would be recorded and present a broad spectrum. The broad spectrum has a similar feature to the spectrum at a higher temperature. Additional errors would be introduced due to the calculation errors and artefacts associated with the implementation of a tomographic algorithm [23, 24]. Therefore, the optical fiber spectrometer might not be a

This is an Accepted Manuscript of Yu, T., Mangalvedhe, K., Francoeur, M., and Bergthorson, J. M. (2024), Dual-range emission spectroscopy for temperature measurement of laminar aluminum dust flames, Combustion and Flame 263. doi: 10.1016/j.combustflame.2024.113421. Licensed under CC BY-NC-ND

proper scientific instrument for emission spectroscopy in dust flames. Soo *et al.* [20] later carried out emission spectroscopy for AlO at the vibrational transition of $B^2\sum^+ \rightarrow X^2\sum^+$, $\Delta v = -1$ by using a 1D spectrometer. Although a 1D measurement was provided, only one location at the upstream of flame front was used to determine temperature due to the optical thickness issue caused by the counter-flow flame. Lomba *et al.* [25] also conducted emission spectroscopy to record a rovibrational AlO spectrum and derive a AlO temperature. The AlO spectrum included more (*i.e.*, three) vibrational transitions compared to the work by Soo *et al.* and should improve the measurement accuracy. Nevertheless, the accuracy is reduced as seen from the large fitting residual presented by the results. Possible reasons for this large fitting residual could be the spatial distribution of AlO structure, variation of quantum efficiency for different wavelengths, and the out-of-focus effect. Note that in most of these works, the methodology for determining the temperature is not clearly introduced. Determination of temperature is not a simple and straightforward implementation [26]. As such, it needs to be clarified mathematically and demonstrated via experiments.

The objective of this work is to develop a dual-range emission spectroscopy system for simultaneous measurement of the continuous spectrum and molecular spectrum of the aluminum dust flame. The continuous spectrum emanates from the liquid phase of $Al_{(L)}$ and/or $Al_2O_{3(L)}$, and the molecular spectrum is from the AlO intermediate combustion product generated mainly in the micro-diffusion flames (MDFs). Based on Planck's law and a library of the theoretical AlO spectrum, the continuous spectrum temperature and AlO temperature are determined. 2D flame imaging is also carried out to monitor the transient flame structure. Major contributions of this work include: 1) the foundations of emission spectroscopy, such as the mathematical formulations, algorithms, signal corrections, accuracy and precision, are introduced in detail; 2) the temperature profiles from the pre-heat zone through to the post-flame zone are presented; 3) the species phase transitions are analyzed by a comparison of the continuous spectrum temperatures against the thermodynamic temperatures of Al and Al_2O_3; 4) the current issues facing emission spectroscopy for metal flame studies are discussed. The measurements enabled by this technique can provide valuable experimental validation data for aluminum combustion simulations, and are beneficial to the development of aluminum combustion models.

This is an Accepted Manuscript of Yu, T., Mangalvedhe, K., Francoeur, M., and Bergthorson, J. M. (2024), Dual-range emission spectroscopy for temperature measurement of laminar aluminum dust flames, Combustion and Flame 263. doi: 10.1016/j.combustflame.2024.113421. Licensed under CC BY-NC-ND

2. Methodology

2.1 Temperatures of aluminum flames

The heterogeneous aluminum dust flame encompasses a number of burning Al fuel droplets, presenting different temperature gradients around each burning Al fuel droplet that vary from the temperature of bulk gas to the MDF temperature in the outer boundary layer, and from the MDF temperature to that of the burning Al fuel droplet, or the residual Al_2O_3 cap, in the region between the MDF and the burning Al fuel droplet. The spatial homogenization of the respective liquid phase temperature, flame temperature, and gas temperature) in a number of temperature gradients within a specific region forms three overarching average temperatures at a specific location of the flame front. A hypothesis for the radial temperature gradients at 5 locations are sketched in Fig. 1 and are labeled by ①-⑤ through the flame front in the overarching temperature profiles at the bottom left. The overarching bulk gas temperature profile is expected to have characteristic pre-heat and reaction zones familiar to homogeneous flames, but three additional characteristic temperatures can also be added. The first is the temperature of the Al fuel particle/droplet. As the initial Al fuel particle moves across the pre-heat zone and over the combustion zone, it will be heated up by conductive heat transfer, and transition into an Al fuel droplet when its temperature is equal to the melting point. As the temperature reaches the boiling point, the liquid phase Al ($Al_{(L)}$) at the outer droplet surface boils, generating Al vapor ($Al_{(v)}$) that diffuses into the MDFs and will be oxidized quickly. The second is the temperature of aluminum combustion products, *i.e.*, Al_2O_3, which are mostly nanometric droplets, or their agglomerates, as well as the residual Al_2O_3 caps that may also have grown by chemical or physical condensation processes. The Al_2O_3 nanometric droplets are formed around the MDFs, with their temperature (not shown in Fig. 1) being close to the in-situ flame temperature or the bulk gas temperature, and different from the temperatures of the Al_2O_3 agglomerates and caps that deposit on the surface of the Al fuel droplet. Due to the small Biot number of aluminum and its oxide, the temperature of the Al_2O_3 agglomerates and caps should be the same as the temperature of the internal Al fuel droplet. Therefore, the temperature profile of the Al_2O_3 agglomerates and caps is overlapped with that of the Al fuel droplet. In the post-flame zone, a thermal balance can be obtained, where the aluminum is burned out and the temperature of the Al_2O_3 product equilibrates with the bulk gas temperature. The third is the flame temperature of intermediate combustion products, which are generated within MDFs around the burning Al fuel droplets. Around each burning Al fuel droplet, the MDF temperature serves as a bridge between the

This is an Accepted Manuscript of Yu, T., Mangalvedhe, K., Francoeur, M., and Bergthorson, J. M. (2024), Dual-range emission spectroscopy for temperature measurement of laminar aluminum dust flames, Combustion and Flame 263. doi: 10.1016/j.combustflame.2024.113421. Licensed under CC BY-NC-ND

temperatures of the Al fuel droplet or the Al_2O_3 cap and the bulk gas, with a maximum value that approaches the adiabatic temperature at the stoichiometry, *i.e.*, $T_{ad,\phi=1}$. According to Glassman's criterion, the flame temperature is limited by the boiling point of Al_2O_3 and/or the Al_2O_3 dissociation [27-30].

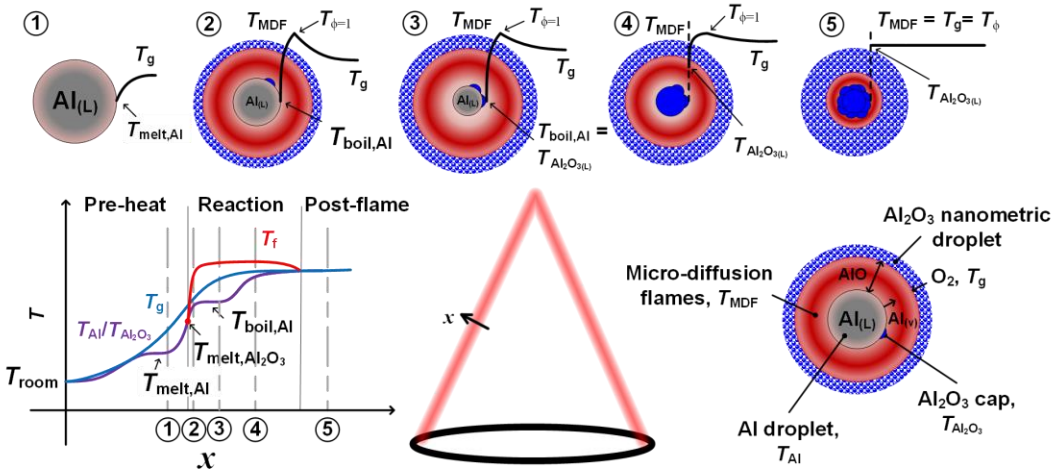

Figure 1. Sketches of the large-scale temperature profiles through the flame and the temperature gradients around the individual aluminum droplets. The red point indicates the location where liquid aluminum is ignited.

2.2 Diagnostics

In this work, a dual-range emission spectroscopy diagnostic system is developed for simultaneous measurements of the continuous spectrum and molecular spectrum with the aim of determining the temperatures of the liquid phase and the flame. In aluminum flames, the continuous spectrum described in [31] is mainly from the liquid phase that includes Al fuel droplets, Al_2O_3 caps, and Al_2O_3 nanometric droplets. The molecular spectrum, *i.e.*, AlO spectrum, is from AlO, which is an intermediate combustion product, and therefore, is an indicator of the gaseous flame front that vanishes beyond the micro-diffusion flame [32]. The bulk gas temperature, *i.e.*, T_g is difficult to measure in dust flames and its diagnostics development will be presented in another work. Figure 2 presents a schematic of the experimental setup. The two types of emissions were first collected and collimated by a f = 200 mm achromat lens. The collimated signals were separated by a beam splitter with a separation ratio of 50/50. Each path of the collimated signals was focused by a f = 100 mm achromat lens at the slit of a spectrometer. The opening of the slit was ~100 μm. A McPherson 218 spectrometer with a 300 lines/mm grating and a Photron SA5

This is an Accepted Manuscript of Yu, T., Mangalvedhe, K., Francoeur, M., and Bergthorson, J. M. (2024), Dual-range emission spectroscopy for temperature measurement of laminar aluminum dust flames, Combustion and Flame 263. doi: 10.1016/j.combustflame.2024.113421. Licensed under CC BY-NC-ND

camera were used to record the continuous spectrum at a visual range of 550 – 700 nm; a SP-2300 spectrometer with a 600 lines/mm grating and a PCO edge 26 camera were used to record the rovibrational AlO spectrum at a range of 480 nm – 540 nm. An additional SA5 camera was used to monitor the transient 2D flame structures. The exposure time of the PCO camera and the two Photron SA5 cameras was 2 μs and 25 μs, respectively. An example image of the flame luminosity is presented in Fig. 2. The white line across the flame front indicates the field of view, which is ~7 mm. The signals from this region are subject to less influence from optical thickness since there are less liquid Al_2O_3 produced and burning Al fuel droplets (*i.e.*, weak flame luminosity) along the recording path. The practical dimension of each pixel of the AlO spectrogram is 4.6 μm, and that of the continuous spectrum is 40 μm. As can be seen from the left graph of Fig. 2, the signal of each pixel is an accumulated intensity of either the AlO spectrum emission from the discrete MDFs or the continuous spectrum emission from the liquid phase, therefore, the temperature derived from each type of signal represents the temperature homogenized within the physical region corresponding to that pixel. Prior to performing experiment, a scale target was captured by the three cameras, which were used to match the measurement locations for different types of signals.

A Bunsen-type burner was used to generate a premixed aluminum/air dust flame. The flame was stabilized above a water-cooled ring (one inch in diameter) with the cooling water at ~285 K. Nitrogen was used as the co-flow and the flow rate is 24 standard liter per minute (SLPM). The aluminum powders (Stockton, CA) used in this work are the same as those employed in a previous study [33] and have an arithmetic mean diameter (d_{10}) of about 3.5 to 3.8 μm. The particle concentration was controlled by the piston speed that is driven by a stepper motor and the dispersed air flow rate. A HeNe laser passing through the space between the ring and the burner nozzle was used to monitor the particle concentration. The basics of the measurement method for particle concentration is described in a previous work [34]. More details about this burner's configuration are given in [33, 35].

This is an Accepted Manuscript of Yu, T., Mangalvedhe, K., Francoeur, M., and Bergthorson, J. M. (2024), Dual-range emission spectroscopy for temperature measurement of laminar aluminum dust flames, Combustion and Flame 263. doi: 10.1016/j.combustflame.2024.113421. Licensed under CC BY-NC-ND

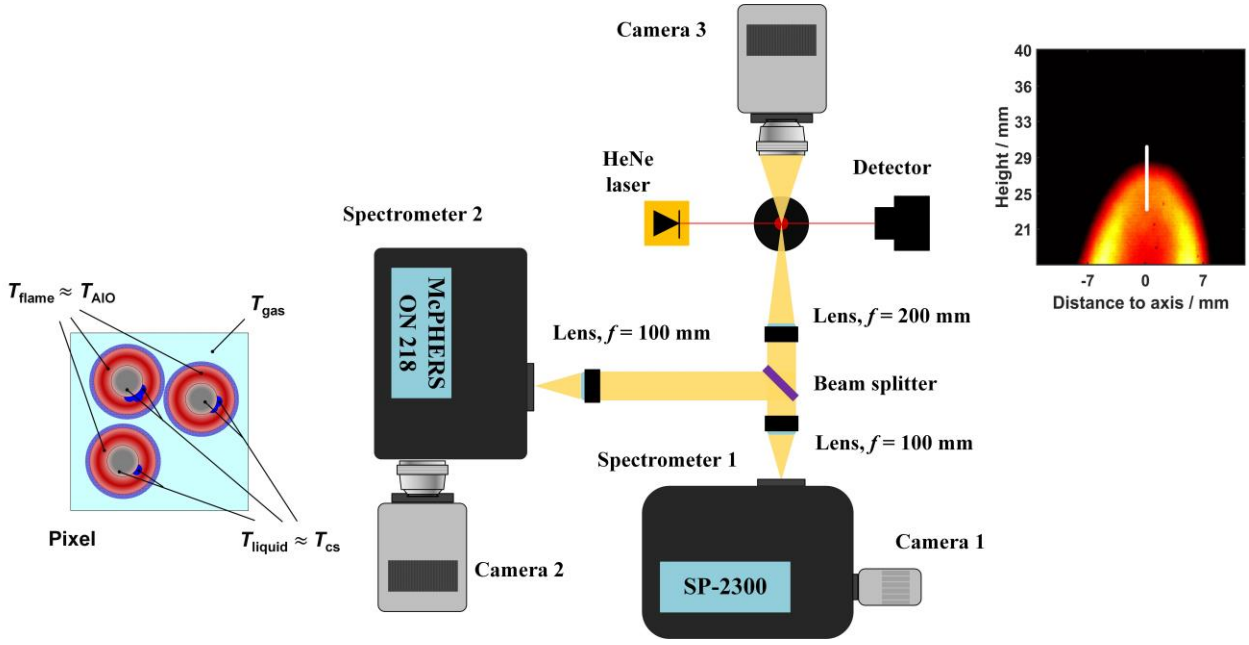

Figure 2. Schematic of the experimental setup for the measurements of continuous spectrum, AlO spectrum, and flame luminosity imaging. The HeNe laser was used to monitor the particle concentration. All the instruments are synchronized by a delay generator.

2.3 Mathematical formulation for temperature determination

The theory for evaluating the continuous spectrum temperature, T_{cs}, is derived based on Planck's law:

$$I_{cs}(\lambda) = \frac{C_1 \varepsilon(\lambda)}{\lambda^5} \frac{1}{e^{C_2/\lambda T_{cs}} - 1} \tag{1}$$

where $I_{cs}(\lambda)$ is the radiative intensity of the continuous spectrum, λ is the wavelength, C_1 and C_2 are the first and second Planck constants, respectively, defined as $C_1 = 2hc^2$ and $C_2 = hc/k$ (h is the Planck constant; c the speed of light; and k the Boltzmann constant), and $\varepsilon(\lambda)$ is the spectral emissivity. The emissivity of a particle whose size is comparable to the wavelength can be approximated as $1/\lambda^2$ in the far infrared band. This relationship is derived based on the low-frequency limit of the dielectric function for a single Lorentz oscillator in the Mie theory [36]. However, in this work, emission is collected in the visible range, and the aluminum combustion produces Al_2O_3 nanometric droplets/particles that are smaller than the measured spectral band [37, 38]. Therefore, this work considers emissivity as $\varepsilon(\lambda) = 4d_p E(m)/\lambda$ based on the Rayleigh approximation [39]. The constant value of the complex refractive index m

This is an Accepted Manuscript of Yu, T., Mangalvedhe, K., Francoeur, M., and Bergthorson, J. M. (2024), Dual-range emission spectroscopy for temperature measurement of laminar aluminum dust flames, Combustion and Flame 263. doi: 10.1016/j.combustflame.2024.113421. Licensed under CC BY-NC-ND

for Al_2O_3 in the visible range [40, 41] results in a constant value of the absorption function, $E(m)$, such that the emissivity is proportional to $1/\lambda$. In the visible range, Eq. (1) can be estimated by Wien's approximation as follows:

$$I_{cs}(\lambda) = \frac{C_1 \varepsilon(\lambda)}{\lambda^5} \frac{1}{e^{C_2/\lambda T_{cs}}} \tag{2}$$

The linearization of Wien's approximation results in:

$$\ln\left(\frac{I_{cs}(\lambda)\cdot\lambda^5}{C_1\varepsilon(\lambda)}\right) = \left(\frac{1}{T_{cs}}\right)\frac{-C_2}{\lambda} \rightarrow y = \frac{1}{T_{cs}}x \tag{3}$$

According to Eq. (3), T_{cs} can be determined by a linear fitting method for the terms of y with respect to x. Figure 3 (a) presents an example of the image of continuous spectrum. This spectrum was obtained from the raw data recorded by the camera and corrected by the background subtraction. The wavelength was calibrated by a Hg-Ar lamp (Ocean Optics), and the intensity was calibrated by using a light source (LS-1-CAL, Ocean Optics). These two calibrations are essential for an accurate linear fitting implementation; without calibrations, there would be larger fitting residuals. The spectral range of continuous spectrum in this work is from 570 nm to 660 nm. As expected, the emission from sodium is observed at ~590 nm, which is consistent with the works in [42, 43]. Figure 3(b) presents an example of the fitting results for the T_{cs} evaluation with 95% prediction interval. To avoid the interference from the sodium emission, the spectral range of 600 nm - 660 nm was chosen to perform the fitting. The uncertainty of the fitting evaluation is ±18 K. The correlation coefficient is consistently larger than 0.95, indicating a reliable temperature evaluation. The emissivity $\varepsilon(\lambda)$ only impacts the y axis in Fig. 3(b). This suggests that once the variation of emissivity with respect to the wavelength is determined, the absolute value of particle diameter d_p does not affect the slope, and thereby, does not change the temperature evaluation.

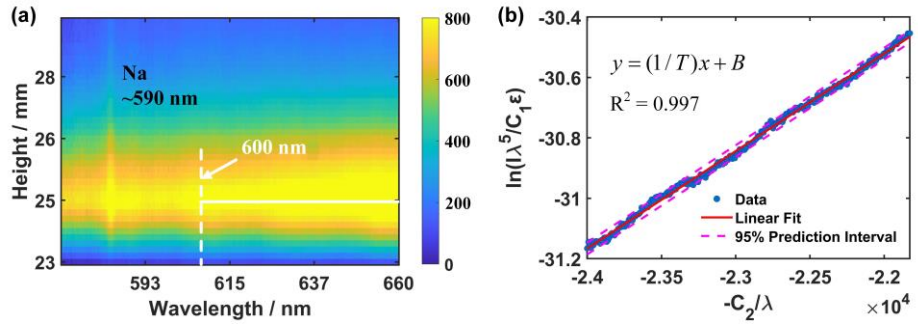

This is an Accepted Manuscript of Yu, T., Mangalvedhe, K., Francoeur, M., and Bergthorson, J. M. (2024), Dual-range emission spectroscopy for temperature measurement of laminar aluminum dust flames, Combustion and Flame 263. doi: 10.1016/j.combustflame.2024.113421. Licensed under CC BY-NC-ND

Figure 3. An example of (a) an image of continuous spectrum with x axis indicating the wavelength and y axis indicating the height above burner (the unit of colorbar is in count); (b) a fitting result for the T_{cs} evaluation based on the spectrum extracted at the height of 25 mm and marked by the white line in Fig. 3(a).

The theory for calculating T_{AlO} is based on a spectral fitting method. Specifically, the convolution of the temperature dependent AlO stick spectra and the instrument function provides a library of theoretical AlO spectrum [11, 44], which is expressed as:

$$I_{AlO}(T,\lambda) = f_{AlO}(T,\lambda) \otimes g(\sigma,\gamma) \tag{4}$$

where $I_{AlO}(T, \lambda)$ denotes a theoretical AlO spectrum, $f_{AlO}(T, \lambda)$ the AlO stick spectrum, and $g(\sigma, \gamma)$ the instrument function modeled by a normalized Voigt function with σ and γ describing the widths of Gaussian and Lorentzian profiles, respectively. The AlO stick spectra used in this work were calculated based on the method described in [45, 46] covering a temperature range between 300 K – 5000 K and the Voigt function was estimated based on the Faddeeva function [47]. In principle, the AlO spectrum $I^{R}_{AlO}(\lambda)$ recorded in experiment is equal to the theoretical AlO spectrum at the same temperature. Therefore, T_{AlO} can be determined by comparing the theoretical and recorded AlO spectra. The curve fitting method for T_{AlO} evaluation is cast into a minimization problem:

$$\min\left\{ f(T) : f(T) = [I^{R}{}_{AlO}(\lambda) - I_{AlO}(T,\lambda)]^2 \right\} \tag{5}$$

Equation (5) was solved by using a nonlinear minimization algorithm proposed by Coleman and Li *et al.* [48, 49]. Figure 4(a) presents an example of an image of the AlO spectrum. Three vibrational transitions, *i.e.*, $\Delta v = 0, -1, -2$ at $B^2\sum^+ \rightarrow X^2\sum^+$ were recorded. Due to the strong flame luminosity, the recorded AlO spectrum was highly interfered by the background, which should be subtracted from the raw data. Figure 4(b) explains the steps for the background subtraction. The data highlighted by the three red ellipses were firstly used to fit a baseline. A second order polynomial function was used, and the fitting curve was validated by assessing the results marked by the orange ellipse. The blue curve in Fig. 4(b) indicates the AlO spectrum after the baseline removal. Prior to performing nonlinear minimization algorithm, the intensity of AlO emission was calibrated by the same light source (LS-1-CAL, Ocean Optics) to that used for continuous spectrum calibration. The wavelength was calibrated by comparing the recorded AlO spectrum and the theoretical AlO stick spectrum. These two calibrations mitigate the effect of the

This is an Accepted Manuscript of Yu, T., Mangalvedhe, K., Francoeur, M., and Bergthorson, J. M. (2024), Dual-range emission spectroscopy for temperature measurement of laminar aluminum dust flames, Combustion and Flame 263. doi: 10.1016/j.combustflame.2024.113421. Licensed under CC BY-NC-ND

spatial variation of collection efficiency and are necessary to take advantage of multiple AlO vibration transitions for improved temperature accuracy. Figure 4(c) presents an example of the fitting result. The residual is less than 10%, suggesting that an accurate temperature measurement is obtained in this work.

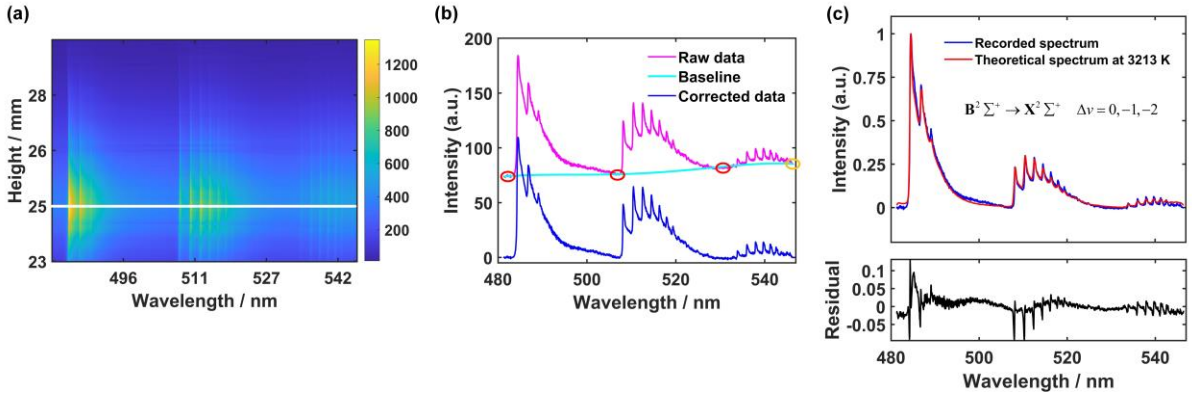

Figure 4. (a) An example of an image of AlO spectrum with x axis indicating the wavelength and y axis indicating the height above burner (the unit of colorbar is in count); (b) steps of background subtraction and (c) a fitting result for the calculation of T_{AlO} along with its fitting residual. The spectrum shown in Figs. 4(b) and (c) is extracted at the height of 25 mm and marked by the white line in Fig. 4(a).

3. Results and Discussion

3.1 1D distributions of emission intensities

The continuous spectrum and AlO spectrum along with 2D flame luminosity imaging provide great insight into the flame structure. The 2D flame luminosity shows the transient flame geometric features, such as the cone shape, flame front region and flame fluctuation, and the two 1D spectra presents the homogenized combustion progress from the upstream to the downstream through the flame front. A comparison between the three types of emission emanated from the 1D region as shown by the white line in Fig. 2 is provided in Fig. 5. The pink curve with squares shows the distribution of flame luminosity (I_{imag}), the blue curve with circles shows the intensity of the continuous spectrum emission (I_{cs}), and the red curve with triangles shows the AlO emission (I_{AlO}). It is found that, as the location goes from the pre-heat zone to post-flame zone, the intensity of I_{AlO} reaches its maximum prior to I_{cs}. This behavior conforms to the formation of AlO within the MDFs, while the Al fuel droplet has a colder temperature

This is an Accepted Manuscript of Yu, T., Mangalvedhe, K., Francoeur, M., and Bergthorson, J. M. (2024), Dual-range emission spectroscopy for temperature measurement of laminar aluminum dust flames, Combustion and Flame 263. doi: 10.1016/j.combustflame.2024.113421. Licensed under CC BY-NC-ND

corresponding to the boiling of the liquid aluminum droplet. The Al fuel droplets and the combustion products of both the Al_2O_3 caps and Al_2O_3 nanometric droplets emit continuous emission whose maximum occurs later than the AlO emission. As discussed in more detail below, the intensity of the continuous spectrum emission is controlled by the emissivity, surface area, and temperature resulting from these three distinct liquid droplets.

In addition, the narrower distributions of I_{cs} and I_{AlO} compared to the flame luminosity intensity demonstrate a smaller depth of field of the emission spectroscopy system compared to the 2D flame imaging system. The depth of field of the emission spectroscopy system was estimated to be ~1.2 mm, which is twice smaller than the laminar flame thickness of 2.8 mm reported by Goroshin *et al.* [35]. Therefore, the Abel transform used in most past works [8, 25] that can introduce additional errors is not necessary in this work. However, it is necessary to point out that the measurement in this work is an accumulation of the signal of the depth of field, which can lead to an overlap of the signals from multiple emitters at different temperatures. This can result in a decreased accuracy and larger uncertainty of the temperature measurements by this system.

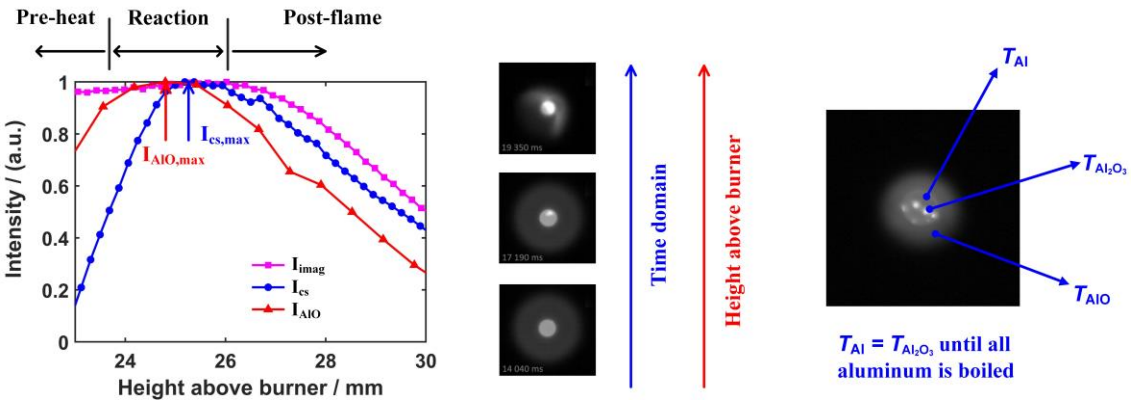

Figure 5. 1D distributions of flame luminosity, continuous spectrum emission and AlO emission for an aluminum flame with 310 g/m^3. The emission intensities were obtained by integrating each spectrum along the spectral direction. A reaction zone is schematically presented by the maximum of AlO and a threshold of continuous spectrum emission at the upstream for the ease of discussion. The images of single aluminum particle combustion are adapted from the work by Glasziou *et al.* [50] and Halter *et al.* [51].

This is an Accepted Manuscript of Yu, T., Mangalvedhe, K., Francoeur, M., and Bergthorson, J. M. (2024), Dual-range emission spectroscopy for temperature measurement of laminar aluminum dust flames, Combustion and Flame 263. doi: 10.1016/j.combustflame.2024.113421. Licensed under CC BY-NC-ND

3.2 Temperature determination for aluminum flames

Figure 6 shows the temperatures of a fuel lean flame and a fuel rich flame. The uncertainties of the temperatures were estimated based on the standard deviation for the selected samples. These selected samples are characterized by the conditions that the movement of the maximum flame luminosity in the 2D flame image is smaller than 0.5 mm. This method is necessary for a reasonable uncertainty quantification; otherwise, the uncertainty would be overestimated because of the flame fluctuation. The dashed lines in Fig. 6 on both sides of the temperature curves indicate the uncertainty, which is around 10%. The standard error of the mean is estimated to be ~62 K. Note that the uncertainty quantification is not directly related to the SNR of the raw data, since the temperature is determined by a fitting method considering the overall effects of the emission spectrum.

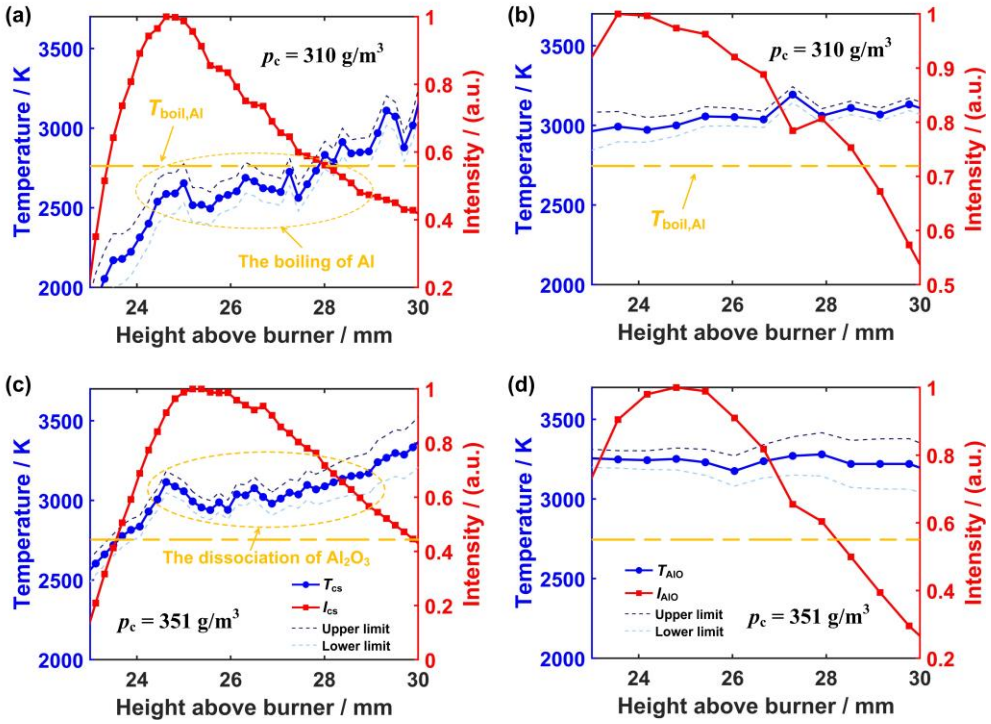

Figure 6. Distributions of (a) the T_{cs} and the continuous emission intensity, and (b) the T_{AlO} and the AlO emission intensity for particle concentration of 310 g/m^3 (ϕ = 0.98). (c) and (d) are counterparts of (a) and (b) for particle concentration of 351 g/m^3 (ϕ = 1.12). The orange dot dash line indicates $T_{boil,Al}$. The stoichiometric value corresponds to a particle concentration at ~320 g/m^3.

This is an Accepted Manuscript of Yu, T., Mangalvedhe, K., Francoeur, M., and Bergthorson, J. M. (2024), Dual-range emission spectroscopy for temperature measurement of laminar aluminum dust flames, Combustion and Flame 263. doi: 10.1016/j.combustflame.2024.113421. Licensed under CC BY-NC-ND

From the pre-heat zone to post-flame zone, it is found that T_{AlO} remains almost constant within a range of 3000 K – 3300 K whereas T_{cs} keeps increasing and eventually reaches the value of T_{AlO}. This observation conforms to the temperature gradient sketches of ②-⑤ presented in Fig. 1. The constant T_{AlO} is consistent with the spatial temperature distribution of the aluminum dust flame simulation reported in [52] and the temperature evolution of a single aluminum particle combustion simulation in terms of time [53]. In addition, the flame temperature estimated from T_{AlO} is larger than the boiling point of aluminum, suggesting a vapor-phase droplet combustion mode [54]. It is also observed that the AlO emission intensity decreases as it goes to the further downstream side while T_{AlO} remains constant. This is because the flame front of the overall flame structure has the most intense combustion reaction of $Al_{(v)}+O_2 \rightarrow AlO^*+O$. The AlO* is an unstable radical and emits photons (*i.e.*, AlO chemiluminescence) quickly. The quantity of $Al_{(v)}$ consumed per unit time denotes the rate of AlO* formation and the rate of photon emission. As it moves downstream of the flame front, the Al fuel droplet burns out and gets smaller. The consumption rate of $Al_{(v)}$ goes down due to a smaller specific surface area, and therefore, the formation rate of AlO* and the chemiluminescence intensity decrease. Meanwhile, the T_{AlO} is constant because of the nature of the MDFs around each individual burning Al fuel droplet. This observation suggests that the overarching flame temperature profile keeps a constant value in the reaction zone, as shown by the sketched temperature profile in Fig. 1.

Figure 6 also shows that the I_{cs} decreases as T_{cs} varies from ~2600 K to ~3250 K. Physically, I_{cs} mainly includes the contributions from three parts: Al fuel droplets ($Al_{(L)}$), the Al_2O_3 caps ($Al_2O_{3(L)}$), and the Al_2O_3 nanometric droplets ($Al_2O_{3(L)}$) around the MDFs. The emission from the $Al_{(L)}$ conforms to the opaque surface theory, and is significantly less than the volumetric emission from the Al_2O_3 cap [55]. It is estimated from past efforts that the emission from the Al_2O_3 cap generated by burning large Al fuel particles (100-400 μm) accounts for 60% of the intensity, the Al fuel droplets accounts for 35%, and the nanometric droplets around the MDFs accounts for the remaining ~5% [56, 57]. In this work, the initial Al fuel particle size is ~3.5 μm. Considering the Al_2O_3 cap in terms of the initial Al fuel particle size reported by Halter *et al.* [51], the Al_2O_3 cap generated by the dust flame of this work is estimated to be ~350 nm (*i.e.*, the oxide cap diameter is ~1/10 of the initial particle diameter). The smaller size of the initial Al fuel particles results in a larger specific surface area, which suggests more $Al_{(L)}$ exposed and more Al_2O_3 nanometric droplets produced around each Al fuel droplet. Therefore, there are more contributions from the $Al_{(L)}$ and Al_2O_3 nanometric droplets to the I_{cs} compared to the works in [56, 57]. However, the Al_2O_3 cap still

This is an Accepted Manuscript of Yu, T., Mangalvedhe, K., Francoeur, M., and Bergthorson, J. M. (2024), Dual-range emission spectroscopy for temperature measurement of laminar aluminum dust flames, Combustion and Flame 263. doi: 10.1016/j.combustflame.2024.113421. Licensed under CC BY-NC-ND

keeps the most dominant contribution to the I_{cs} due to its volumetric emission property. The lag of T_{cs} compared to T_{AlO} in the combustion region shown in Fig. 6 suggests that the T_{cs} is dominated by the Al fuel droplets and the Al_2O_3 caps, rather than the Al_2O_3 nanometric droplets, since the temperature of the Al_2O_3 nanometric droplets is expected to be close to the flame temperature. According to Zhang *et al.* [58] and Lynch *et al.* [57], the emissivity of aluminum is consistently larger than 0.1, which is 500-1000 times stronger than that of Al_2O_3 nanometric droplets. Additionally, since the nanometric droplets are formed around the MDFs, the produced aluminum oxide cap cannot compensate the volumetric loss of the Al fuel particles/droplets as the aluminum burns away. Therefore, the noticeable decrease of emissivity during the continuous reactions from $Al_{(L)}$ to Al_2O_3 cap and Al_2O_3 nanometric droplets result in the decease of I_{cs} while T_{cs} stays constant or increases.

In addition, a temperature plateau in the distribution of T_{cs} is observed at ~2600 K for the fuel lean condition. This temperature is close to the boiling point of aluminum, $T_{boil,Al}$ [59]. Thus, this temperature plateau is attributed to the boiling process of aluminum, during which the aluminum at the burning Al fuel droplet surface keeps boiling and causes a constant temperature of the liquid phase. Furthermore, a temperature gradient change is observed at ~3000 K for the fuel rich condition. To explain the presence of this gradient change, the thermal equilibrium calculation [60] was carried out by assigning the temperature values. Figure 7 presents the mole fractions for the involved species of fuel lean, stoichiometric, and fuel rich conditions. As can be seen, there is a large amount of AlO and Al remained or re-generated as the temperature exceeds 3000 K, meanwhile, the mole fraction of $Al_2O_{3(L)}$ is decreasing. In addition, there is no $Al_2O_{3(g)}$ produced in all conditions. This indicates that the slower temperature rise after the gradient change is a result of the dissociation of $Al_2O_{3(L)}$, and the dissociation is a reversible reaction and its extent becomes intense as the temperature increases. On the other hand, Figure 7 also suggests that the AlO is oxidized into $Al_2O_{3(L)}$ completely once the temperature drops below 3000 K. Therefore, the oxidation of AlO and the subsequent condensation also maintain the oxide's temperature constant as it transports to the bulk gas that has a relatively lower temperature.

This is an Accepted Manuscript of Yu, T., Mangalvedhe, K., Francoeur, M., and Bergthorson, J. M. (2024), Dual-range emission spectroscopy for temperature measurement of laminar aluminum dust flames, Combustion and Flame 263. doi: 10.1016/j.combustflame.2024.113421. Licensed under CC BY-NC-ND

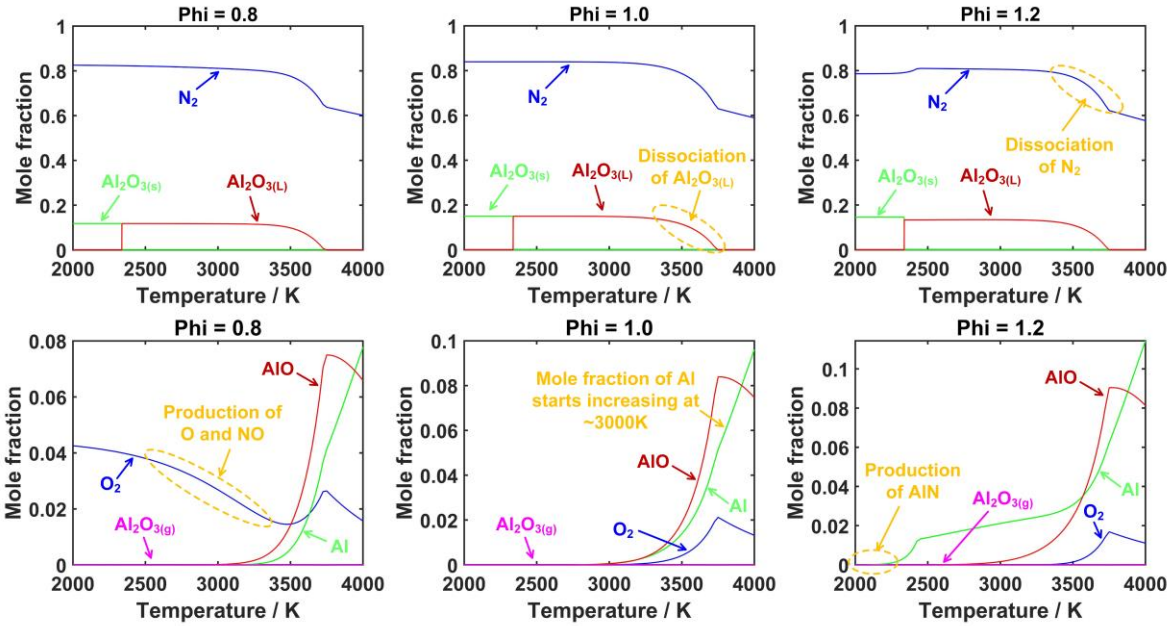

Figure 7. Mole fractions of the species obtained from thermal equilibrium calculation for aluminum combustion in air.

The T_{cs} and T_{AlO} of the aluminum dust flames at particle concentrations within the range from ~290 g/m^3 to ~360 g/m^3 were also evaluated. Table 1 shows the particle concentrations and the corresponding air flow rates. In order to investigate the relationship of diverse temperatures in aluminum flame and avoid the effects from combustion process, the temperature at HAB = 30 mm were extracted since this location is at the post flame region where all chemical reactions have finished. Figure 8(a) shows the temperatures with respect to the particle concentration. As can be seen, a thermal balance is obtained, and T_{cs} and T_{AlO} are identical. Considering the uncertainties of T_{cs} and T_{AlO}, the temperatures are almost constant with an average of ~3200 K and a fluctuation of ±205 K. The adiabatic aluminum flame temperatures at different particle concentrations, *i.e.*, $T_{ad,\phi}$, were calculated using the thermal equilibrium calculation [60]. If $T_{ad,\phi}$ is assumed to be true, the measurement error should be quantified as ~350 K. However, the accuracy is underestimated since the overarching flame temperature should be lower than $T_{ad,\phi}$ due to the radiation heat transfer from flames and the homogenization effect of the temperature gradients (see Fig. 1). In order to analyze the relationship of the thermodynamic temperatures, a comparison of T_{cs}, T_{AlO}, $T_{boil,Al}$, $T_{ad,\phi}$, $T_{ad,\phi=1}$, $T_{d,Al2O3}$, and the boiling point of Al_2O_3 is also provided. The dissociation temperature

This is an Accepted Manuscript of Yu, T., Mangalvedhe, K., Francoeur, M., and Bergthorson, J. M. (2024), Dual-range emission spectroscopy for temperature measurement of laminar aluminum dust flames, Combustion and Flame 263. doi: 10.1016/j.combustflame.2024.113421. Licensed under CC BY-NC-ND

($T_{d,Al2O3}$) was calculated based on the work by Beckstead [61], which is ~3992 K. But it is necessary to point out that the dissociation temperature tends to occur at a higher temperature when the oxygen partial pressure becomes lower [62]. As can be seen from Fig. 8(a), there is a minor variation between $T_{ad,\phi}$ and $T_{ad,\phi=1}$ as the condition varies from fuel lean to fuel rich condition. Therefore, the maximum of the MDF temperature should be limited by some physical and chemical process so that the value keeps constant. Glassman's theory suggests that the metal flame temperature is limited by the boiling and dissociation of the metal oxide [27-30]. As can be seen from Fig. 8(a), the $T_{ad,\phi}$ is consistently smaller than the bottom limit of the boiling point of Al_2O_3 by ~50 K. In addition, the average values of both T_{cs} and T_{AlO} at HAB = 30 mm are approximately equivalent, and are smaller than $T_{ad,\phi}$ by ~350 K. Therefore, the flame temperature should not be limited by the boiling point of Al_2O_3. In order to determine the reason of the minor variation between $T_{ad,\phi}$ and $T_{ad,\phi=1}$, another calculation was conducted by assigning the temperature values to be the same as the average of the evaluated temperatures. Figure 8(b) and (c) present the mole fractions of Al, AlO, O_2, and $Al_2O_{3(L)}$ at the adiabatic flame temperature and the experimentally averaged temperature, respectively. As can be seen, the assigned lower temperatures compared to the adiabatic flame temperatures result in a larger mole fraction of $Al_2O_{3(L)}$ and a weaker extent of dissociation (refer to Fig. 7). In addition, the stoichiometric condition generates the maximum concentration of $Al_2O_{3(L)}$, and as the combustion condition becomes richer there are less $Al_2O_{3(L)}$ and more AlO remained in the thermal equilibrium condition. Therefore, it can be concluded that the minor variation between $T_{ad,\phi}$ and $T_{ad,\phi=1}$ is caused by the dissociation process of Al_2O_3.

Table 1. The particle concentrations and the corresponding air flow rates of the aluminum combustion conditions. The particle concentration was altered by changing the piston speed when the air flow rates were the same.

Particle concentration (g/m^3)	290	310	322	328	336	346	350	356
Air flow rate (SLPM)	13.2	14.4	15.6	14.4	15.6	18.0	16.8	18.0

This is an Accepted Manuscript of Yu, T., Mangalvedhe, K., Francoeur, M., and Bergthorson, J. M. (2024), Dual-range emission spectroscopy for temperature measurement of laminar aluminum dust flames, Combustion and Flame 263. doi: 10.1016/j.combustflame.2024.113421. Licensed under CC BY-NC-ND

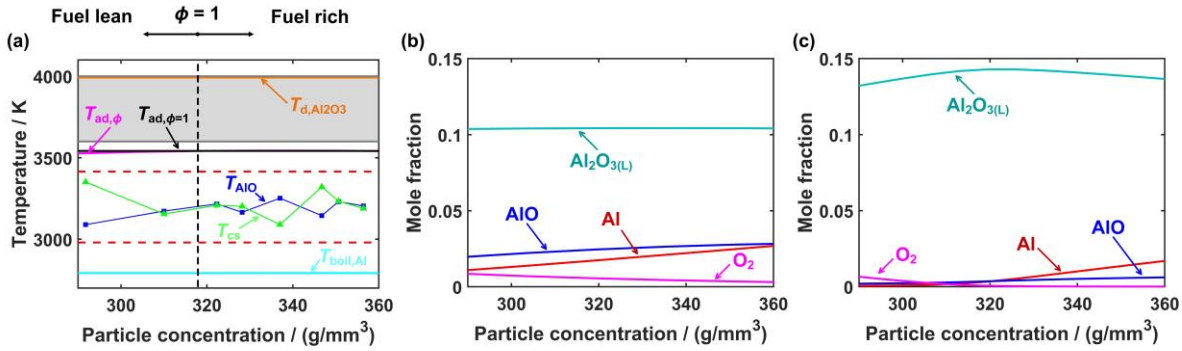

Figure 8. (a) A comparison of T_{cs}, T_{AlO}, the boiling point of Al ($T_{boil,Al}$) [59], the adiabatic temperature ($T_{ad,\phi}$) [60], the adiabatic temperature at the stoichiometry ($T_{ad,\phi=1}$) [60], and the dissociation temperature of Al_2O_3 ($T_{d,Al2O3}$) [61]. The shaded region is the boiling point of Al_2O_3 with the uncertainty range reported by Brewer and Searcy [63]. The melting point of Al_2O_3 is 2327 K [64] and is not shown. (b), (c) Mole fractions of the species of interest at the adiabatic flame temperature and the experimentally averaged temperature (*i.e.*, ~3200 K), respectively.

3.3 Interference of the multi-phase medium

As the Al fuel droplet is burning, its size decreases, thus influencing the choice of the formulation for the spectral emissivity. To assess the influence of emissivity on the temperature evaluation, numerical studies were performed by assuming that $\varepsilon(\lambda)$ is proportional to $1/\lambda^{\alpha}$. It was found that the temperature was increased by ~600 K as α varies from 1 to 0 (α = 0 indicates a grey body assumption), and decreased by ~ 400 K as α varies from 1 to 2. Figure 8 shows that a thermal equilibrium between T_{cs} and T_{AlO} can be obtained when α = 1. In addition, the temperature plateau and the temperature gradient change of the T_{cs} distributions shown in Fig. 6 conform with the temperature of the boiling point of Al and that the $Al_2O_{3(L)}$ starts to dissociate. This suggests that the Rayleigh approximation for the wavelength dependence of the spectral emissivity in the measured spectral band results in a reasonable temperature determination, and verifies the effectiveness of the technique in determining temperatures of aluminum dust flames. However, the emissivity may vary in different zones depending on the size of the Al fuel droplet, the composition of the liquid phase, and the topology of the Al fuel droplet and the Al_2O_3 cap. Therefore, at some locations $\varepsilon(\lambda)$ may not vary proportionally to $1/\lambda$, causing a large measurement error. Accordingly, the temperature plateau and the temperature gradient change shown in Fig. 6 might take place at the same temperature,

This is an Accepted Manuscript of Yu, T., Mangalvedhe, K., Francoeur, M., and Bergthorson, J. M. (2024), Dual-range emission spectroscopy for temperature measurement of laminar aluminum dust flames, Combustion and Flame 263. doi: 10.1016/j.combustflame.2024.113421. Licensed under CC BY-NC-ND

and they can be attributed to a single process of either the boiling of Al or the dissociation of Al_2O_3, depending on the true temperatures.

The interference signal caused by the scattering of Al fuel droplets, the Al_2O_3 caps, and the Al_2O_3 nanometric droplets is a general and inevitable issue of the diagnostics for dust flames. As a result, the signals of interest are recorded along with the scattered radiation, which actually originates from the reaction zone that has stronger emission intensities and higher temperatures. Therefore, the temperature derived at the reaction zone should be close to the practical value, whereas the temperatures derived at other zones would be overestimated. Note that the signal absorption by the multi-phase medium does not influence the temperature determination because T_{cs} is determined based on the slope of the linear fitting and T_{AlO} is determined based on the temperature dependent shape of AlO spectrum, rather than the emission intensities. The measurements can be improved by developing a tomographic model as proposed in [65] and by performing 3D reconstruction for the emission distribution with the consideration of scattering, following by evaluating temperatures. In addition, high spatial resolution imaging and emission spectroscopy are necessary to identify individual Al fuel droplets and recognize Al_2O_3 caps.

4. Summary

A dual-range emission spectroscopy technique that can measure simultaneously the continuous spectrum and the rovibrational AlO spectrum was developed. The signal correction routine, which is essential for accurate fitting implementation, was described in detail. A linear fitting method and a nonlinear minimization algorithm were introduced for the determination of continuous spectrum temperature T_{cs} and AlO temperature T_{AlO}. It was found that the correlation coefficient of the linear fitting for T_{cs} is consistently larger than 0.95 and the uncertainty of the fitting evaluation is around ±18 K. The fitting residual of the nonlinear minimization algorithm for T_{AlO} is less than 0.1. The accuracy of the technique is at least 350 K, and the uncertainty is approximately 10%. The results suggest that the T_{cs} represents the homogenized temperature of the three distinct liquid phases, *i.e.*, the Al fuel droplets and Al_2O_3 caps and any Al_2O_3 nanometric droplets formed in or around the MDFs. The T_{AlO} represents the homogenized temperature of the MDFs within the measurement volume. Furthermore, the phase transitions, such as the boiling of Al and the dissociation of Al_2O_3, are observed from the determined liquid phase temperature. The maximum of the MDF temperature is limited by the dissociation reaction, and the extent of dissociation reaction becomes intense as the

This is an Accepted Manuscript of Yu, T., Mangalvedhe, K., Francoeur, M., and Bergthorson, J. M. (2024), Dual-range emission spectroscopy for temperature measurement of laminar aluminum dust flames, Combustion and Flame 263. doi: 10.1016/j.combustflame.2024.113421. Licensed under CC BY-NC-ND

temperature increases. Due to the MDFs formed around individual burning Al fuel droplets, the flame temperature stays nearly constant in the reaction zone. It is observed that, in the post-flame region where the temperatures are expected to equilibrate, the temperatures from the AlO spectrum and the continuous spectrum agree closely, providing confidence in the choice of the Rayleigh approximation for the wavelength dependence of the emissivity. In addition, the flame temperature does not deviate noticeably from the adiabatic temperature at the stoichiometry as the particle concentration (*i.e.*, equivalence ratio) varies. Such measurements can provide valuable validation data for the simulations, which are beneficial to the development of aluminum combustion modeling frameworks.

Declaration of competing interest

The authors declare that they have no known competing financial interests or personal relationships that could have appeared to influence the work reported in this paper.

Acknowledgments

This work is funded by the grants from Fonds de recherche du Québec – Nature et technologies (Funding Reference No. 298413) and Canadian Space Agency (Funding Reference No. 21FAMCGA17). Additional funding is from the Student Development Scholarship provided by Shanghai Jiao Tong University. M.F. acknowledges the support of the Natural Sciences and Engineering Research Council of Canada (NSERC) (Funding Reference No. RGPIN-2023-03513). The authors would like also to acknowledge Prof. Fabien Halter at ICARE- CNRS, Université d'Orléans for the valuable discussions on Aluminum single particle combustion.

References

[1] T.J. Wallington, J.E. Anderson, D.J. Siegel, M.A. Tamor, S.A. Mueller, S.L. Winkler, O.J. Nielsen, Sustainable Mobility, Future Fuels, and the Periodic Table, J. Chem. Educ. 90 (2013) 440-445.
[2] D.L. Sanchez, K. Fingerman, C. Herbert, S. Uden, Policy Options for Deep Decarbonization and Wood Utilization in California's Low Carbon Fuel Standard, Front. clim. 3 (2021) 665778.
[3] J.M. Bergthorson, Recyclable metal fuels for clean and compact zero-carbon power, Prog. Energy Combust. Sci. 68 (2018) 169-196.
[4] S. Goroshin, I. Fomenko, J.H.S. Lee, Burning velocities in fuel-rich aluminum dust clouds, Symp. (Int.) Combust. 26 (1996) 1961-1967.
[5] N. Glumac, H. Krier, T.I.M. Bazyn, R. Eyer, Temperature measurements of aluminum particles burning in carbon dioxide, Combust. Sci. Technol. 177 (2005) 485-511.
[6] P. Monkhouse, On-line diagnostic methods for metal species in industrial process gas, Prog. Energy Combust. Sci. 28 (2002) 331-381.

This is an Accepted Manuscript of Yu, T., Mangalvedhe, K., Francoeur, M., and Bergthorson, J. M. (2024), Dual-range emission spectroscopy for temperature measurement of laminar aluminum dust flames, Combustion and Flame 263. doi: 10.1016/j.combustflame.2024.113421. Licensed under CC BY-NC-ND

[7] F. Sewerin, J. Finke, A Eulerian population balance/Monte Carlo approach for simulating laminar aluminum dust flames, Particuology 88 (2024) 323-343.
[8] S. Goroshin, J. Mamen, A. Higgins, T. Bazyn, N. Glumac, H. Krier, Emission spectroscopy of flame fronts in aluminum suspensions, Proc. Combust. Inst. 31 (2007) 2011-2019.
[9] P.E. Bocanegra, V. Sarou-Kanian, D. Davidenko, C. Chauveau, I. Gökalp, Studies on the burning of micro-and nanoaluminum particle clouds in air, Progress in Propulsion Physics 1 (2009) 47-62.
[10] F. Fuest, R.S. Barlow, J.-Y. Chen, A. Dreizler, Raman/Rayleigh scattering and CO-LIF measurements in laminar and turbulent jet flames of dimethyl ether, Combust. Flame 159 (2012) 2533-2562.
[11] C. Yang, H. Tang, G. Magnotti, Picosecond Kerr-gated Raman spectroscopy for measurements in sooty and PAH rich hydrocarbon flames, Proc. Combust. Inst. 38 (2021) 1797-1804.
[12] P. Bucher, R.A. Yetter, F.L. Dryer, T.P. Parr, D.M. Hanson-Parr, PLIF species and ratiometric temperature measurements of aluminum particle combustion in O2, CO2 and N2O oxidizers, and comparison with model calculations, Symp. (Int.) Combust. 27 (1998) 2421-2429.
[13] G. Vilmart, N. Dorval, R. Devillers, Y. Fabignon, B. Attal-Trétout, A. Bresson, Imaging aluminum particles in solid-propellant flames using 5 kHz LIF of Al atoms, Materials 12 (2019) 2421.
[14] C. Schulz, B.F. Kock, M. Hofmann, H. Michelsen, S. Will, B. Bougie, R. Suntz, G. Smallwood, Laser-induced incandescence: recent trends and current questions, Appl. Phys. B 83 (2006) 333-354.
[15] A. Omrane, F. Ossler, M. Aldén, Temperature measurements of combustible and non-combustible surfaces using laser induced phosphorescence, Exp. Therm Fluid Sci. 28 (2004) 669-676.
[16] A. Omrane, F. Ossler, M. Aldén, J. Svenson, J.B.C. Pettersson, Surface temperature of decomposing construction materials studied by laser-induced phosphorescence, Fire Mater. 29 (2005) 39-51.
[17] B. Tian, C. Zhang, Y. Gao, C. Tung Chong, S. Hochgreb, 2D 2-Colour time-Resolved laser induced incandescence sizing of ultra-fine soot particles in a methane diffusion flame, Proc. Combust. Inst., (2022).
[18] J. Huang, S. Li, D. Sanned, L. Xu, S. Xu, Q. Wang, M. Stiti, Y. Qian, W. Cai, E. Berrocal, M. Richter, M. Aldén, Z. Li, A detailed study on the micro-explosion of burning iron particles in hot oxidizing environments, Combust. Flame 238 (2022) 111755.
[19] J.I. Vovchuk, N.I. Poletaev, The temperature field of a laminar diffusion dust flame, Combust. Flame 99 (1994) 706-712.
[20] M. Soo, S. Goroshin, N. Glumac, K. Kumashiro, J. Vickery, D.L. Frost, J.M. Bergthorson, Emission and laser absorption spectroscopy of flat flames in aluminum suspensions, Combust. Flame 180 (2017) 230-238.
[21] M.D. Ruesch, A.J. McDonald, G.C. Mathews, S.F. Son, C.S. Goldenstein, Characterization of the influence of aluminum particle size on the temperature of composite-propellant flames using CO absorption and AlO emission spectroscopy, Proc. Combust. Inst. 38 (2021) 4365-4372.
[22] J. Zhang, Z. Xia, O.T. Stein, L. Ma, F. Li, Y. Feng, Z. Zhang, A. Kronenburg, Combustion characteristics of aluminum particle jet flames in a hot co-flow, Chem. Eng. J. 442 (2022) 135876.
[23] S.J. Grauer, K. Mohri, T. Yu, H. Liu, W. Cai, Volumetric emission tomography for combustion processes, Prog. Energy Combust. Sci. 94 (2023) 101024.
[24] W. Cai, C.F. Kaminski, Tomographic absorption spectroscopy for the study of gas dynamics and reactive flows, Prog. Energy Combust. Sci. 59 (2017) 1-31.
[25] R. Lomba, P. Laboureur, C. Dumand, C. Chauveau, F. Halter, Determination of aluminum-air burning velocities using PIV and Laser sheet tomography, Proc. Combust. Inst. 37 (2019) 3143-3150.
[26] S. Knapp, S. Kelzenberg, A. Raab, E. Roth, V. Weiser, Emission Spectroscopy of the Combustion Flame of Aluminium/Copper Oxide Thermite, Propell. Explos. Pyrot. 44 (2019) 9-17.
[27] I. Glassman, Metal combustion Processes, Report No. 473, Aeornautical Engineering Laboratory, Princeton University, New Jersey, USA, 1959.
[28] T.A. Steinberg, D.B. Wilson, F. Benz, The combustion phase of burning metals, Combust. Flame 91 (1992) 200-208.
[29] I. Glassman, Comment on “The combustion phase of burning metals” by T. A. Steinberg, D. B. Wilson, and F. Benz, Combust. Flame 93 (1993) 338-342.
[30] T.A. Steinberg, D.B. Wilson, F. Benz, Response to Comment by I. Glassman on" The Combustion Phase of Burning Metals", Combust. Flame 93 (1993).
[31] G.-A. Valley, R. Telescope, Basics of Radio Astronomy, Jet Propulsion Laboratory, Mission Execution and Automation Section, Customer Integration Services Group, (1998).
[32] P. Bucher, R.A. Yetter, F.L. Dryer, T.P. Parr, D.M. Hanson-Parr, E.P. Viceni, Flames structure measurement of single, isolated aluminum particles burning in air, Symp. (Int.) Combust. 26 (1996) 1899-1908.

This is an Accepted Manuscript of Yu, T., Mangalvedhe, K., Francoeur, M., and Bergthorson, J. M. (2024), Dual-range emission spectroscopy for temperature measurement of laminar aluminum dust flames, Combustion and Flame 263. doi: 10.1016/j.combustflame.2024.113421. Licensed under CC BY-NC-ND

[33] F. Blais, P. Julien, J. Palecka, S. Goroshin, J.M. Bergthorson, Effect of Initial Reactant Temperature on Flame Speeds in Aluminum Dust Suspensions, Combust. Sci. Technol. 194 (2022) 1513-1526.
[34] P. Julien, M. Soo, S. Goroshin, D.L. Frost, J.M. Bergthorson, N. Glumac, F. Zhang, Combustion of Aluminum Suspensions in Hydrocarbon Flame Products, J. Propul. Power 30 (2014) 1047-1054.
[35] S. Goroshin, M. Bidabadi, J.H.S. Lee, Quenching distance of laminar flame in aluminum dust clouds, Combust. Flame 105 (1996) 147-160.
[36] C.F. Bohren, D.R. Huffman, Absorption and scattering of light by small particles, John Wiley & Sons, 1998.
[37] C.-y. Tu, X. Chen, Y.-k. Li, B.-c. Zhang, C.-s. Zhou, Experimental study of Al agglomeration on solid propellant burning surface and condensed combustion products, Def. Technol. 26 (2023) 111-122.
[38] P. Bucher, R.A. Yetter, F.L. Dryer, E.P. Vicenzi, T.P. Parr, D.M. Hanson-Parr, Condensed-phase species distributions about Al particles reacting in various oxidizers, Combust. Flame 117 (1999) 351-361.
[39] J. Seki, T.J.A. Yamamoto, S. Science, Amorphous interstellar grains: Wavelength dependence of far-infrared emission efficiency, Astrophys. Space Sci 72 (1980) 79-86.
[40] F. Gervais, Aluminum Oxide (Al2O3), in: E.D. Palik (Ed.), Handbook of Optical Constants of Solids, Academic Press, Boston, 1998, pp. 761-775.
[41] I.H. Malitson, F.V. Murphy, W.S. Rodney, Refractive Index of Synthetic Sapphire, J. Opt. Soc. Am. 48 (1958) 72-73.
[42] Q. Wang, J. Huang, H. Liu, Z. Qin, W. Cai, 3D particle sizing, thermometry and velocimetry of combusting aluminized propellants, Combust. Flame 247 (2023) 112500.
[43] M. Soo, P. Julien, S. Goroshin, J.M. Bergthorson, D.L. Frost, Stabilized flames in hybrid aluminum-methane-air mixtures, Proc. Combust. Inst. 34 (2013) 2213-2220.
[44] T.W. Haller, Thermometry in high pressure gases using spontaneous Raman scattering, PhD dissertation, The University of Texas at Austin, (2021).
[45] A.T. Patrascu, S.N. Yurchenko, J. Tennyson, ExoMol molecular line lists – IX. The spectrum of AlO, Mon. Not. R. Astron. Soc. 449 (2015) 3613-3619.
[46] A.T. Patrascu, C. Hill, J. Tennyson, S.N. Yurchenko, Study of the electronic and rovibronic structure of the X 2Σ+, A 2Π, and B 2Σ+ states of AlO, J. Chem. Phys. 141 (2014).
[47] S.M. Abrarov, B.M. Quine, Efficient algorithmic implementation of the Voigt/complex error function based on exponential series approximation, Appl. Math. Comput. 218 (2011) 1894-1902.
[48] T.F. Coleman, Y. Li, An interior trust region approach for nonlinear minimization subject to bounds, SIAM J. Optim. 6 (1996) 418-445.
[49] Y. Li, T. Coleman, On the convergence of reflective newton methods for large-scale nonlinear minimization subject to bounds, Math. Program. 67 (1994) 189-224.
[50] V. Glasziou, G. Legros, C. Chauveau, S. Courtiaud, F. Halter, Temperature measurement during the combustion of a single aluminium particle, 29th International Colloquium on the Dynamics of Explosions and Reactive Systems, Siheung, South Korea, 2023.
[51] F. Halter, V. Glasziou, H. Keck, G. Legros, C. Chauveau, Experimental investigation of ignition temperatures of aluminum particles, 13th United States National Combustion Meeting, College station, TX, United States, 2023.
[52] D.-H. Han, H.-G. Sung, A numerical study on heterogeneous aluminum dust combustion including particle surface and gas-phase reaction, Combust. Flame 206 (2019) 112-122.
[53] J. Liu, Q. Chu, D. Chen, On Modeling the Combustion of a Single Micron-Sized Aluminum Particle with the Effect of Oxide Cap, ACS Omega 6 (2021) 34263-34275.
[54] J.M. Bergthorson, S. Goroshin, M.J. Soo, P. Julien, J. Palecka, D.L. Frost, D.J. Jarvis, Direct combustion of recyclable metal fuels for zero-carbon heat and power, Appl. Energy 160 (2015) 368-382.
[55] J. Harrison, M.Q. Brewster, Analysis of thermal radiation from burning aluminium in solid propellants, Combust. Theory Model. 13 (2009) 389-411.
[56] J. Harrison, Q. Brewster, Infrared Emitted Intensity Measurements from Burning Aluminum Droplets in Solid Propellants, Combust. Sci. Technol. 181 (2008) 18-35.
[57] P. Lynch, H. Krier, N. Glumac, Emissivity of aluminum-oxide particle clouds: application to pyrometry of explosive fireballs, J. Thermophys. Heat Trans. 24 (2010) 301-308.
[58] K. Zhang, K. Yu, Y. Liu, Y. Zhao, Effect of surface oxidation on emissivity properties of pure aluminum in the near infrared region, Mater. Res. Express 4 (2017) 086501.
[59] R.C. Weast, CRC handbook of chemistry and physics, Cleveland, Ohio : CRC Press, 1978.
[60] B.J. McBride, Computer program for calculation of complex chemical equilibrium compositions and applications, NASA Lewis Research Center, 1996.

This is an Accepted Manuscript of Yu, T., Mangalvedhe, K., Francoeur, M., and Bergthorson, J. M. (2024), Dual-range emission spectroscopy for temperature measurement of laminar aluminum dust flames, Combustion and Flame 263. doi: 10.1016/j.combustflame.2024.113421. Licensed under CC BY-NC-ND

[61] M.W. Beckstead, A summary of aluminum combustion, Internal Aerodynamics in Solid Rocket Propulsion, RTO-EN-023, Rhode-Saint-Genèse, Belgium, 2002.
[62] R. Reed, V. Calia, Review of aluminum oxide rocket exhaust particles, 28th Thermophysics Conference, American Institute of Aeronautics and Astronautics, 1993.
[63] L. Brewer, A.W. Searcy, The Gaseous Species of the Al-Al2O3 System1,2,3, J. Am. Chem. Soc. 73 (1951) 5308-5314.
[64] S.J. Schneider, Cooperative determination of the melting point of alumina, Pure Appl. Chem. 21 (1970) 115-122.
[65] T. Yu, Z. Li, C. Ruan, F. Chen, X. Lu, W. Cai, Development of an absorption-corrected method for 3D computed tomography of chemiluminescence, Meas. Sci. Technol. 30 (2019) 045403.